Available online at www.sciencedirect.com

SciVerse ScienceDirect

Proceedings of the Combustion Institute xxx (2012) xxx–xxx

Proceedings of the Combustion Institute

www.elsevier.com/locate/proci

Effects of low air pressure on radiation-controlled rectangular ethanol and *n*-heptane pool fires

Ran Tu, Jun Fang *, Yong-ming Zhang, Jun Zhang, Yi Zeng

State Key Laboratory of Fire Science, University of Science and Technology of China, Hefei, Anhui 230026, PR China

Abstract

Experiments on rectangular ethanol and *n*-heptane pool fires were conducted at different altitudes in Hefei (99.8 kPa) and Lhasa (66.5 kPa). The burners tested had the same fuel area of 900 cm^2, but with aspect ratio of long side to short side ($n = l/w$) varied from 1 and 8. The individual and combined influences of low pressure and aspect ratio on burning rate, temperature, puffing frequency, flame height and radiation for the two fuels were interpreted and formulated. First, burning rate was found to be proportional to ambient air pressure under radiation control, the main reason is that radiative heat flux decreased with pressure due to the pressure affecting the soot absorption coefficient. Flame temperature slightly increased, leading to higher flame puffing frequency at low pressure. Flame height was almost insensitive to pressure as $H \propto p^0$. Second, for aspect ratio n, flame temperature was constant and independent of fuel type and burner shape. With increasing n, burner wall temperature increased at the long side, and decreased drastically at the short side, especially $n = 8$. This was attributed to the change of flame tilt and heating of the burner side, caused by variation of entrainment motion. Flame puffing frequency was found to increase with n as a function of $f \sim \sqrt{(\Delta T/T_\infty)(n+1)/2\sqrt{n}}$. The flame was observed to split into small clusters by enhanced asymmetric entrainment, and H decreased with increasing n as $H \sim (1/\sqrt{n})^{2/5}\dot{Q}^{4/15}$. Considering fuel differences, with increasing n, the burning rate of the ethanol pool fire decreased, and *n*-heptane showed the opposite trend.

Keywords: Low pressure; Aspect ratio; Burning rate; Flame characteristics; Radiation controlled

1. Introduction

Low air pressure has been shown to affect pool fire burning behavior by experimental studies [1–6], from which empirical correlations have been obtained. The burning rate was found to be $\dot{m}'' \sim p^{\alpha}$, where $\alpha \sim 1.3$ in Wieser et al. [1]. Similar results were reported by Fang et al. [2] and Li et al. [4], but a larger α was suggested in Hu et al. [5]. In 2011, Fang et al. [6] used more burners with side sizes from 4 to 33 cm, α was found to vary in three ranges, −0.4 to 1, 1–1.45, 1 by conduction, convection and radiation heat feedback-control, respectively. With the same square burner at low air pressure, flame temperature and puffing frequency showed little increase.

Theoretical modeling of air pressure influences on fires has mainly focused on confined laminar or jet fires at elevated pressures [7–9]. However, laminar flame theory cannot fully explain turbulent fire dynamic mechanisms. The principal work for turbulent pool fires has been the pressure

* Corresponding author. Fax: +86 551 3606430.
E-mail address: fangjun@ustc.edu.cn (J. Fang).

1540-7489/$ - see front matter © 2012 The Combustion Institute. Published by Elsevier Inc. All rights reserved.
http://dx.doi.org/10.1016/j.proci.2012.06.036

Nomenclature

$\dot{m}''$	mass burning rate per unit area (g/m^2 s)	ΔH_g	heat of gasification (kJ/g)
$\dot{q}''$	heat flux (kW/m^2)	H	flame height (m)
Q	heat release rate or HRR (kW)	U_{f0}	vapor velocity at source (m/s)
ρ	density (kg/m^3)	f	flame puffing frequency (Hz)
D	equivalent burner diameter length (m)	g	acceleration of gravity (m/s^2)
l	long side length of rectangular burner (m)	c_p	specific heat capacity for constant pressure
w	width or short side length of rectangular burner (m)	σ	Stephan–Boltzmann constant
S	area (m^2)	*Subscripts*	
p	pressure (kPa)	f	flame
ΔH_c	heat of combustion (kJ/g)	∞	ambient
		s	fuel surface

modeling and radiation fire modeling of De Ris et al. [10,11], based on scale principles. These models provide an important experimental guide, but cannot be directly applied for comparison of same-scale pool fires in two different pressure environments.

Compared with idealized circular or square pool fires, rectangular or line fires are more common in fire engineering [12–14]. Because of the irregular shapes, burning behavior shows obvious asymmetry relative to axisymmetric pool fires. Moreover, soot and radiation differences between experimental fuels were ignored by some prior works. These differences should be considered in practical engineering.

In this paper, rectangular pool fires with aspect ratio $n = l/w$ varying from 1 to 8 were studied under 99.8 kPa (Hefei) and 66.5 kPa (Lhasa) pressures. Phenomenological models of low pressure and aspect ratio effects on burning rates, flame height, puffing frequency and radiation were established and validated by experimental results. Ethanol and *n*-heptane pool fires were chosen for good repeatability and their different soot production abilities.

2. Experiments

The experimental setup is shown in Fig. 1. Fuel parameters [6,15] are listed in Table 1. Experiments were conducted in EN54 standard fire test rooms with dimensions 10 m long, 7 m wide and 4 m high [16] at the two locations respectively.

Four rectangular burners with the same 900 cm^2 fuel area but different aspect ratios were used: $n = 1$ (30 cm/30 cm); $n = 2$ (42.4 cm/21.2 cm); $n = 4$ (60 cm/15 cm); $n = 8$ (84.8 cm/10.6 cm). Burners were made of steel plate, 2 mm thick with inner depth 4 cm. The height of the liquid fuel surface above the pan bottom in each test was 1.4 cm (ethanol: 1000 g; *n*-heptane: 860 g). The fire source was set on the center of the test room floor.

Electronic balance (Mettler Toledo, Excellence-Plus XP) was used to record mass loss with precision 0.01 g. Temperatures were obtained by Type K armored thermocouples with diameter 0.5 mm, uncertainty within 0.75%, and response time less than 1 s [17]. In the figure, $T1$ and $T3$ show temperatures at long and short exterior side walls, respectively, and $T2$ shows interior fuel temperature. Axial flame temperature was measured by thermocouple array $T4$–$T10$. Two radiant heat flux sensors (Captec, TS-30) of resolution 0.0015 kW/m^2 were placed 5 cm above the burner surface and 1.5 m away from burner center at the long and short sides, respectively. A high-speed camera (Fastec, Trouble Shooter) with 250 frames per second was used to record the visible flame information. A thermal infrared imager (SAT, HY 6850) with temperature range −40 to 2000 °C and spectral range 8–14 μm were used to capture flame thermal images, and IR

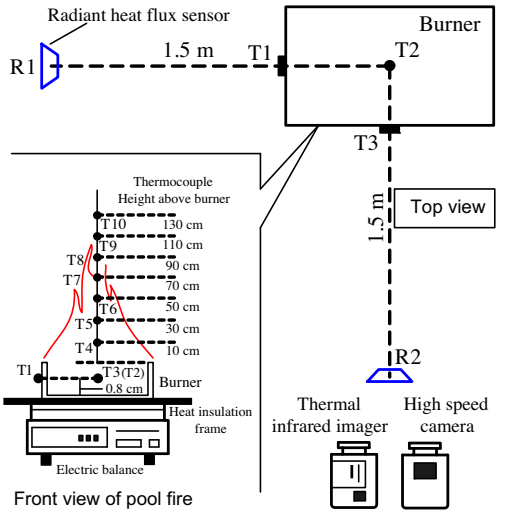

Fig. 1. Sketch of experimental setup.

Table 1
Properties of ethanol and n-heptane.

Fuel material	Molecular formula	Density (g/cm^3)	Boiling point (°C)		Heat of combustion (kJ/g)	Soot yield (g/g)
			Hefei	Lhasa		
Ethanol	C_2H_6O	0.789	78.3	67.0	29.64	0.012
n-Heptane	C_7H_{16}	0.680	98.5	89.0	47.97	0.037

temperature was further calibrated by the data of thermal couple. Any use of trade names is for descriptive purposes only.

In contrast to air pressure, similar ambient temperatures and humidities were applied at the two locations (Lhasa: 18 ± 2.0 °C, $50 \pm 4\%$; Hefei: 20 ± 2.0 °C, $55 \pm 3\%$). Each test was repeated several times to ensure reproducible results within permitted error ranges.

3. Results and analysis

3.1. Burning rate

The burning rates of pool fires in the steady burning stage (from the linear fit shown in Fig. 2) are shown in Fig. 3(a). Figure 3(b) shows $\dot{m}''_{Lhasa}/\dot{m}''_{Hefei}$ vs. n at the two locations. For the same burner and fuel, $\dot{m}''_{Lhasa}/\dot{m}''_{Hefei}$ is approximately equal to the ratio of air pressures, and is unaffected by aspect ratio n. A similar result was reported by Fang et al. [6] for square pool fires with diameter exceeding 20 cm. However, no quantitative theory has been given to explain the correlation. Here, based on radiation fire modeling [10] and experimental correlation, a quantitative theoretical analysis is as follows.

The burning rate corresponds to three types of heat feedback and is radiation-dominated when $D > 20$ cm [18], i.e. $\dot{m}'' \sim \dot{q}''_{rad}/\Delta H_g$. $\dot{q}''_{rad}$ is simplified as [10]:

$$\dot{q}''_{rad} = \sigma T_f^4 [1 - \exp(-\kappa_s L)] \quad (1)$$

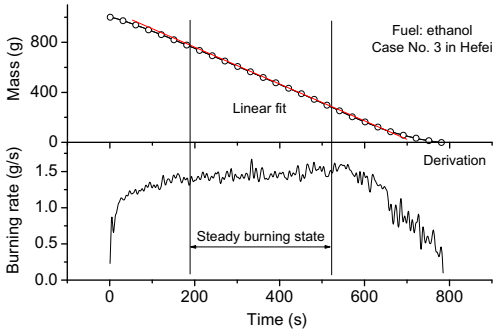

Fig. 2. Experimental data of mass variation. Burning rate $\dot{m}''$ is determined by derivation of mass loss in steady burning state.

First, based on the hypothesis of radiation fire modeling that by holding $D \cdot p^2 = \text{constant}$, κ_s ($\sim p^2 \sim D^{-1}$) is the soot absorption coefficient and ($L \sim D$) beam length [10]. T_f is flame temperature considered insensitive to fire scale and ambient pressure, as confirmed in Section 3.2. Since $\kappa_s L$ remains invariant, $\dot{q}''_{0,rad} = \dot{q}''_{d,rad}$, and thus $\dot{m}''_0 = \dot{m}''_d$, where subscript 0 denotes the prototype fire at 1 atm, and d is for the model fire under decreased pressure.

Second, burner scale varies with pressure due to $D \cdot p^2 = \text{constant}$ in radiation fire modeling. Therefore, to compare $\dot{m}''$ at different pressures with the same scale burner, scale transformation is done subsequently.

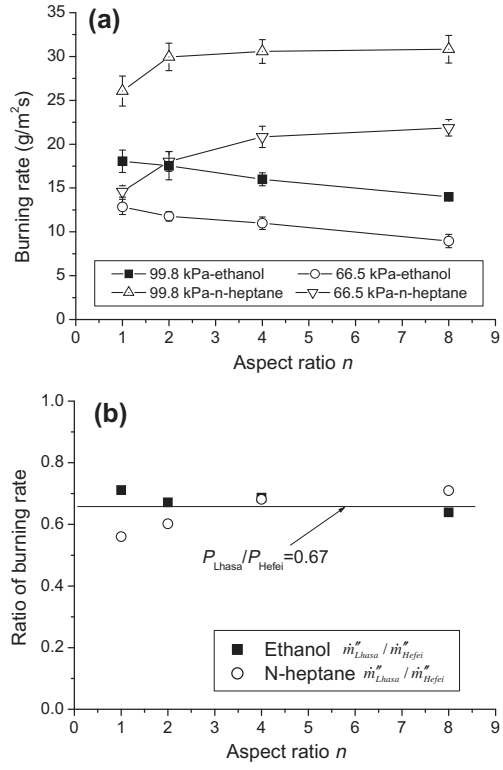

Fig. 3. Burning rates of pool fires (a), and ratio of $\dot{m}''_{Lhasa}/\dot{m}''_{Hefei}$ (b), with various aspect ratios in Hefei (99.8 kPa) and Lhasa (66.5 kPa).

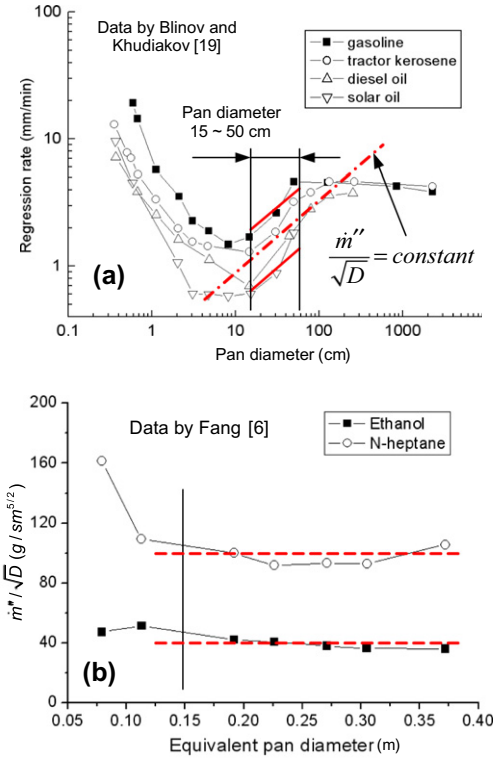

Fig. 4. Burning rate for liquid pools from Blinov and Khudiakov, $\dot{m}''/\sqrt{D} \approx constant$ between diameter 15 and 50 cm (a), which is also validated by Fang's study (b).

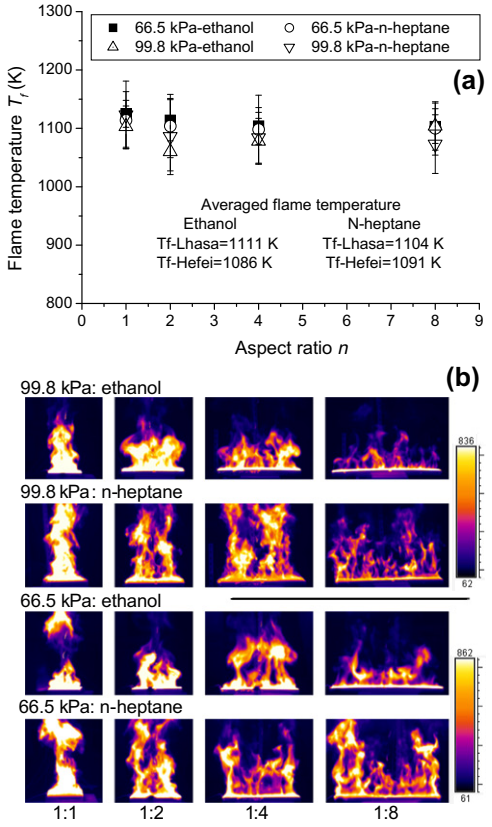

Fig. 5. Flame temperatures (a), and infrared images (b; unit: °C) in Hefei (99.8 kPa) and Lhasa (66.5 kPa) with various aspect ratios.

Table 2
Correlations of parameters under different pressure conditions.

1 atm		Transformed Pressure decreased	Correlations
p_0	p_0	p_d	$p_d = \beta p_0$
D_0	D_d	D_d	$D_d = D_0/\beta^2$
$\dot{m}_0''$	$\dot{m}_{0t}''$	$\dot{m}_d''$	$\dot{m}_d'' = \dot{m}_0''\dot{m}_{0t}'' = \dot{m}_0''/\beta = \dot{m}_d''/\beta$

From the results of Blinov et al. [19] under normal pressure, $\dot{m}''/\sqrt{D}$ is nearly constant for fuels with D from 15 to 50 cm (Fig. 4). This is an important experimental result for scale transformation, and also reflects the non-dimensional heat release rate $\dot{Q}^*$:

$$\frac{\dot{m}''}{D^{1/2}} \sim \dot{Q}^* = \frac{\dot{Q}}{\rho_\infty T_\infty c_p \sqrt{g} D^2} \sim \text{constant}, \ 15\ \text{cm} < D < 50\ \text{cm} \quad (2)$$

Assuming diameters of the prototype fire (1 atm) and model fire (low pressure) are D_0 and D_d, respectively, and the scale-transformed prototype fire (1 atm) has burning rate $\dot{m}_{0t}''$ and diameter D_d (the same scale as the model fire). The following relation should ultimately exist:

$$\left.\begin{array}{l} p_d D_d^{1/2} = p_0 D_0^{1/2}, \dot{m}_d'' = \dot{m}_0'' \ \text{(radiation fire modeling)} \\ \dot{m}_0''/D_0^{1/2} = \dot{m}_{0t}''/D_d^{1/2} \ \text{(experimental correlation)} \end{array}\right\} \Rightarrow \frac{\dot{m}_d''}{p_d} = \frac{\dot{m}_{0t}''}{p_0} \ or \ \dot{m}'' \propto p \quad (3)$$

Table 2 summarizes correlations between prototype, scale-transformed prototype and model fires under two different pressures.

For the aspect ratio effect, it is not expected that ethanol and *n*-heptane pool fire burning rates develop oppositely with increasing n, as shown in Fig. 3(a). This will be explained in Section 3.3 by combining temperature and flame height data.

3.2. Flame and burner wall/fuel temperature

Flame temperature T_f, defined as constant peak temperature in the continuous flame region of turbulent diffusion flames, is shown in Fig. 5. Figure 5(a) shows that T_f is nearly independent of the shape or material of the fuel source, but

is affected by pressure. Averaged T_f measured under 99.8 kPa and 66.5 kPa was about 1089 and 1108 K, respectively. Although the difference of T_f between the two locations is not obvious, T_f in Lhasa was slightly higher, mainly because of less radiative heat loss of the flame at low pressure, and weaker ambient air entrainment cooling for lower air density [4,6].

For burner wall temperature T_w and fuel temperature T_{fuel}, the influence of pressure is not obvious as shown in Fig. 6(a). The aspect ratio effect upon T_w is shown in Fig. 6(b) typically using ethanol pool fires in Lhasa, which has the similar trend of *n*-heptane. Figure 6(b) reveals that with increasing n, T_w at the long side is increased, while at the short side, a sharp decrease appears at $n = 8$. The influence of n on T_{fuel} is not obvious; a comparison is given in Fig. 6(c) for burning time = 200 s. To further understand the effect of n on T_w, entrainment theory was used for explanation.

As shown in Fig. 7, with large aspect ratio, significant inward flame tilt near the short side by strong airflow entrainment was observed (Fig. 7(b)). Assuming air entrainment velocity V, η indicates the burner characteristic length parallel to the entrainment velocity. Horizontal and vertical pressure differences of entrained air by vortices pumping are $\Delta p_H \sim \rho_f V^2$ and $\Delta p_V \sim \rho_\infty g\eta$ [20], giving

$$\frac{\Delta p_H}{\rho_\infty} \sim \frac{\rho_f}{\rho_\infty} V^2 \sim \frac{\Delta p_V}{\rho_\infty} \sim g\eta \Rightarrow V \sim g^{1/2}\eta^{1/2} \qquad (4)$$

So, for a rectangular pool fire, there is larger V on the short side than on the long side (Fig. 7(a), $V_w > V_l$). With increasing n, l, therefore increased V_w and flame inclination, the flame receded from the rim of the short side wall (Fig. 7(b)), and temperature decreased. For the flame near the long side (Fig. 7(c)), the pushing of inward air became weaker because of the narrow fire source. The flame was even closer to the rim, increasing the temperature as shown in Fig. 6(b).

3.3. Flame image characteristic

Digital image processing was used to calculate flame height H and flame puffing frequency f. Flame height was obtained from 60-s sequenced flame images from the steady burning state, using the mean flame height definition of Zukoski et al. [21]. Frequency was obtained by a high-speed camera using the fast Fourier transform method.

3.3.1. Flame puffing frequency

The frequency of a circular pool fire was demonstrated to be $f \propto 1/\sqrt{D}$ [22]. Cetegen et al. studied the oscillatory behavior of planar buoyant plumes using a rectangular nozzle [23], by keeping the long side length 200 mm and varying nozzle widths from 20 to 70 mm. The frequency of the hot plume without chemical reaction was shown to be:

$$f = (1 - \rho_p/\rho_\infty)^{0.45} g^{0.45} w^{-0.55} V_p^{0.1} \qquad (5)$$

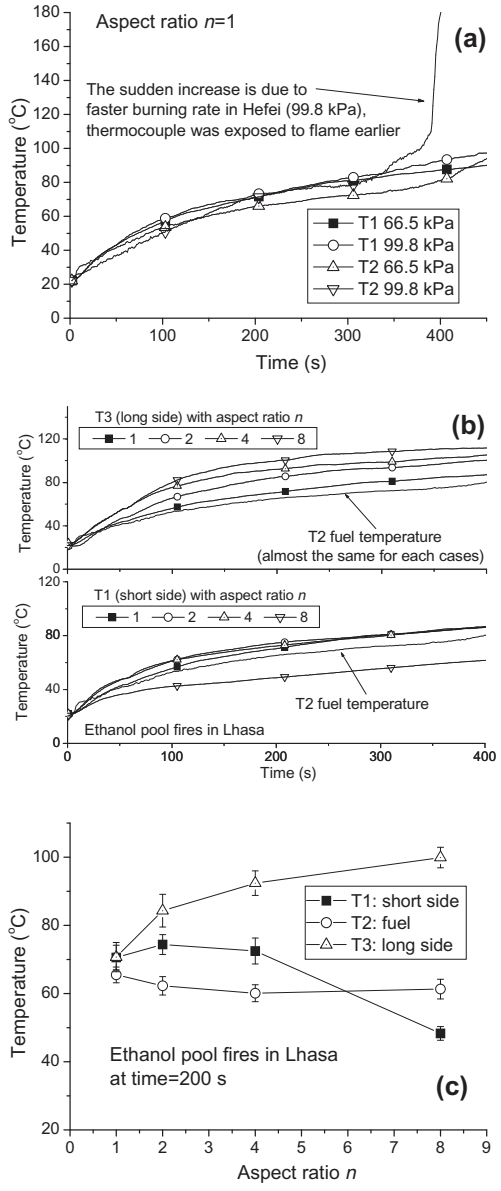

Fig. 6. Burner exterior wall and fuel temperatures of ethanol pool fires: influence of pressure on wall and fuel temperature (a); influence of aspect ratio on temperature for ethanol pool fires in Lhasa (66.5 kPa) at long side wall and short side wall (b); comparison of temperatures at a given time (c).

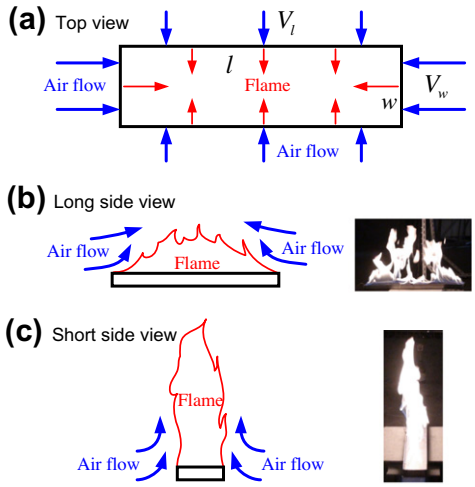

Fig. 7. Flame shape and air flow at enlarged aspect ratio.

where ρ_p is the hot plume density, and V_p the vertical plume velocity. This shows that frequency has a strong dependence on ρ_p/ρ_∞ (or T_∞/T_p) and w. For a circular pool fire with large Ri number, $Ri = \frac{(\rho_\infty-\rho_f)gD}{\rho_f U_{f0}^2}$, f could be simplified as [20]:

$$f = C\sqrt{\rho_\infty/\rho_f - 1}\cdot\sqrt{\frac{g}{D}} = C\sqrt{\frac{\Delta T}{T_\infty}\cdot\frac{g}{D}} \tag{6}$$

where C is a proportion factor. For the rectangular burner, a hydraulic diameter defined as $D^* = 2w\cdot l/(w+l)$ is introduced. Considering fuel area $S_s = w\cdot l = constant$ and $l/w = n$, substituting D^* into Eq. (6) gives:

$$f = C'\sqrt{\frac{\Delta T}{T_\infty}\cdot\frac{g}{D^*}} = C'\sqrt{\frac{\Delta T}{T_\infty}\cdot\frac{g}{S_s}\cdot\frac{(n+1)}{2\sqrt{n}}} \tag{7}$$

First, Eq. (7) shows that for the pressure effect, because of stronger buoyancy convection induced by higher T_f, f is slightly higher at Lhasa than at Hefei (independent of fuel type). This is illustrated by Fig. 8(a).

Second, for the aspect ratio effect, Eq. (7) indicates that $f \propto \sqrt{(n+1)/2\sqrt{n}}$ when p remains constant. Figure 8(b) shows experimental and predicted values of f/f_0 vs. n. Here, subscript 0 is for the square burner. The correlation predicted by Eq. (7) appears to scale with experimental data.

3.3.2. Flame height

Flame height is expressed as $H/D = 3.7\dot{Q}^{*2/5} - 1.02$ [24], as $\dot{Q}^* = \frac{\pi D^2\dot{m}''\Delta H_c}{4\rho_\infty T_\infty c_p\sqrt{gD}D^2}$ $\sim \dot{m}''/p\sqrt{D}$ and $\dot{m}'' \propto p$ shown above, giving $\dot{Q}^* \sim p^0$, and thus $H/D \sim p^0$. This means that air pressure has no conspicuous influence on flame height as Fig. 9 shows.

With increasing n, H became lower for both ethanol and n-heptane pool fires. However, for ethanol, the decrease of H was greater. A qualitative analysis is given below.

Taking the 99.8 kPa condition as an example, for a square pool fire, the assumed flame height and theoretical HRR are H_0 and $\dot{Q}_0 = S_s\dot{m}''\Delta H_c$ respectively. For a rectangular pool fire, they are H and $\dot{Q} = \delta\dot{Q}_0$. δ is a coefficient based on experimental data above; $\delta = 0.77 \sim 1.18$. The flame height of an axisymmetric pool fire is classically expressed as Eq. (8) [24]. The classical correlation of H for a rectangular fire was suggested by Hasemi et al. as Eq. (9) [14]:

$$Square: H_0 = 0.235\dot{Q}_0^{2/5} - 1.02D \tag{8}$$

$$Rectangular: H = 0.035(\delta\dot{Q}_0/l)^{2/3}, \quad n > 3 \tag{9}$$

So, for the same fuel area condition, there is the approximation:

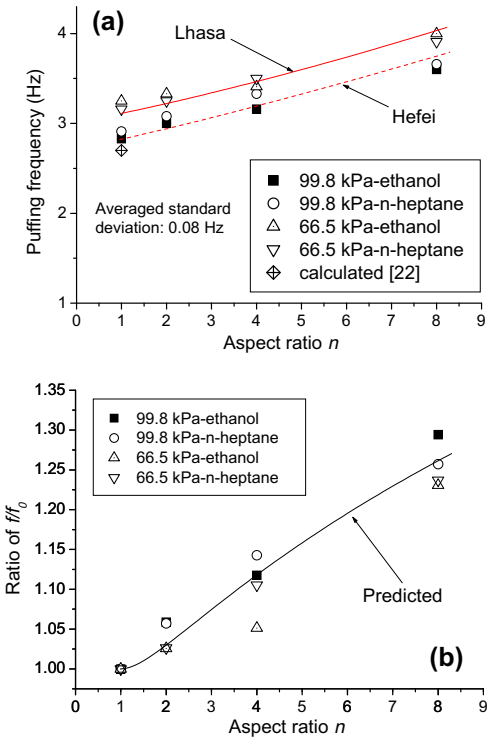

Fig. 8. Experimental puffing frequencies (a) and f/f_0 (b) vs. aspect ratio of rectangular pool fires in Hefei (99.8 kPa) and Lhasa (66.5 kPa).

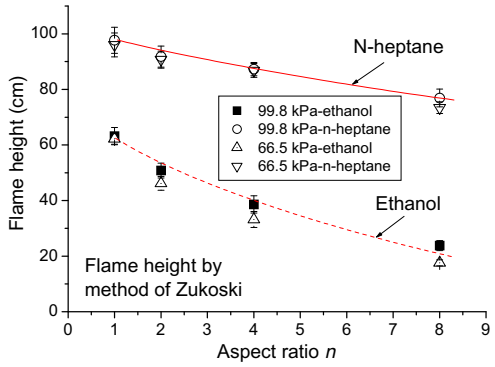

Fig. 9. Flame heights of pool fires with aspect ratio in Hefei (99.8 kPa) and Lhasa (66.5 kPa).

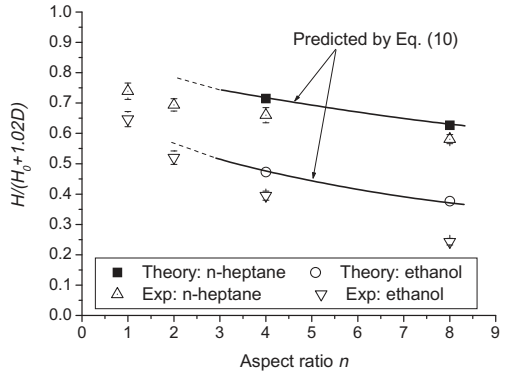

Fig. 10. Experimental and predicted flame heights correlated with aspect ratio and heat release rate.

$$\frac{H}{1.02D+H_0}=0.149\left(\frac{1}{\sqrt{nS_s}}\right)^{2/5}\cdot\delta^{2/3}\dot{Q}_0^{4/15},\ n>3 \tag{10}$$

Eq. (10) shows that H decreases with increasing n, and the larger $\dot{Q}_0$ is, the more slowly H decreases with n. Compared with ethanol, n-heptane has a greater burning rate, meanwhile, ΔH_c is nearly two times that of ethanol, leading to a larger $\dot{Q}_0$, so H of an ethanol pool fire decreases faster with increasing n. Eq. (10) is validated by Fig. 10.

We now return to the question in Section 3.1, regarding the opposite development of ethanol and n-heptane pool fire burning rates vs. n at the two locations. Figure 10 indicates the decrease of H vs. n, so does $L\sim H$ in Eq. (1). Since T_f remains nearly constant, $\dot{q}''_{rad}$ also decreases with increasing n. This effect will degrade the burning rate $\dot{m}''$. Considering that H-ethanol decreases faster than n-heptane as shown above, the degradation effect on ethanol is therefore stronger. On the other hand, for the rectangular burner, the increasing T_w vs. n at the long side wall cannot be ignored, which enhances the burning rate. Finally, $\dot{m}''$ vs. n is determined by the coupling effects of increasing wall heating and decreasing radiation heat feedback, which produces the opposite development for the two fuels.

3.4. Radiation heat flux

The radiant heat of a pool fire depends on the radiation fraction and burning rate $\dot{q}''\propto\chi_r\dot{m}''$. The radiation fraction, $\chi_r=\dot{Q}_{rad}/\dot{Q}$, is proven to be independent of pressure when $D\cdot p^2=constant$ according to radiation fire modeling [10]:

$$\chi_r=\dot{Q}_{rad}/\dot{Q}=\frac{S_f\sigma T_f^4[1-\exp(-\kappa_s L)]}{S_s\Delta H_c\dot{m}''}\sim p^0 \tag{11}$$

Considering that the radiation fraction shows no dependence on pan diameter between 7.6 and 122 cm [25], χ_r should be almost the same for low pressure and normal pressure, i.e., $\chi_{r-Lhasa}=\chi_{r-Hefei}$ for a mid-scale pool fire. For the radiation heat flux measured at the same position in Hefei and Lhasa, combining Eq. (3) gives

$$\dot{q}''_{Lhasa}/\dot{q}''_{Hefei}=\dot{m}''_{Lhasa}/\dot{m}''_{Hefei}=p_{Lhasa}/p_{Hefei} \tag{12}$$

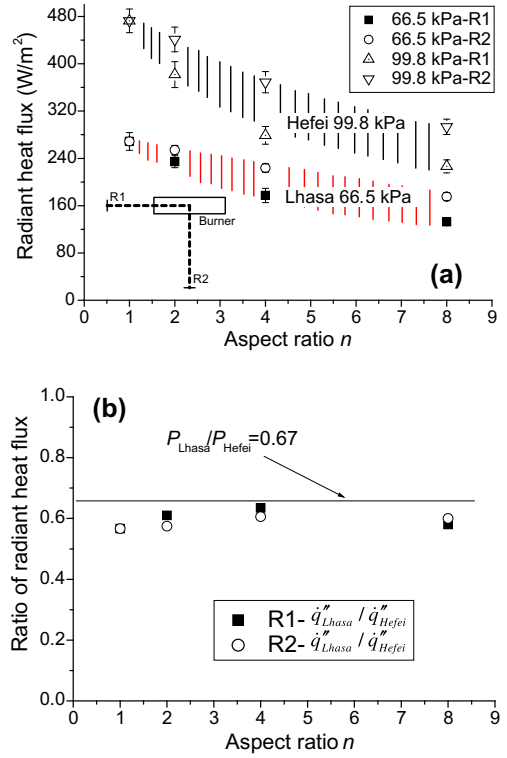

Fig. 11. Comparison of radiant heat flux of ethanol pool fires in Hefei (99.8 kPa) and Lhasa (66.5 kPa).

Figure 11 compares the radiant heat flux of ethanol pool fires at the two locations. Figure 11(a) shows that for the same measuring position,

$\dot{q}''$ in Hefei is much larger than in Lhasa, and $\dot{q}''$ facing the long side of the burner (R2) is larger than that facing the short side (R1). This is because of the different geometric radiation coefficients and stronger extinction of soot through the long side. The $\dot{q}''_{Lhasa}/\dot{q}''_{Hefei}$ is shown in Fig. 11(b), which agrees with the prediction of Eq. (12).

4. Conclusions

Rectangular ethanol and *n*-heptane pool fires with the same fuel area but different aspect ratios were conducted under 99.8 and 66.5 kPa conditions. Major results are summarized as follows:

(1) Burning rate and radiant heat flux were proportional to air pressure $\dot{m}'' \sim \dot{q}'' \propto p$ under radiation-controlled, which was interpreted by formulas based on radiation fire modeling and experimental correlation.
(2) At low air pressure, flame temperature slightly increased, leading to higher flame puffing frequency. Flame height was nearly independent of pressure.
(3) Regarding the aspect ratio effect, flame temperature was constant and independent of burner shape. Burner wall temperature increased at the long side, and drastically decreased at the short side for $n = 8$, owing to variation of entrainment movement.
(4) Flame puffing frequency was found to be $f \propto \sqrt{(\Delta T/T_\infty)(n+1)/2\sqrt{n}}$, which reflects the combined effects of p and n. Flame height decreased with increasing n as $H \sim (\frac{1}{\sqrt{n}})^{2/5}\dot{Q}_0^{4/15}$.
(5) For the fuel difference, with increasing n, flame heights of the ethanol pool fire decreased at a greater extent; burning rate of the ethanol pool fire decreased, whereas n-heptane showed the opposite trend, it is caused by the coupling effects of wall heating and radiation heat feedback.

Acknowledgments

This research was supported by the National Natural Science Foundation of China (No. 51036007) and National Key Technology R&D Program (No. 2011BAK03B02). Fang Jun was supported by China NSFC 51074147, the Chinese Universities Scientific Fund and the Fund of Key Laboratory of Microgravity of Institute of Mechanics of CAS. The authors express sincere appreciation to Dr. John L. De Ris of FM Global for his generous help and suggestions on this work.

References

[1] D. Wieser, P. Jauch, U. Willi, *Fire Saf. J.* 29 (1997) 195–204.
[2] J. Fang, C.Y. Yu, R. Tu, L.F. Qiao, Y.M. Zhang, J.J. Wang, *J. Hazard. Mater.* 154 (2008) 476–483.
[3] A. Shinotake, S. Koda, K. Akita, *Combust. Sci. Technol.* 43 (1985) 85–97.
[4] Z.H. Li, Y.P. He, H. Zhang, J. Wang, *Proc. Combust. Inst.* 32 (2009) 2481–2488.
[5] X.K. Hu, Y.P. He, Z.H. Li, J. Wang, *Proc. Combust. Inst.* 33 (2011) 2607–2615.
[6] J. Fang, R. Tu, J.F. Guan, J.J. Wang, Y.M. Zhang, *Fuel* 90 (2011) 2760–2766.
[7] J.M. Most, P. Mandin, J. Chen, P. Joulain, D. Durox, A.C. Fernandez-Pello, *Proc. Combust. Inst.* 26 (1996) 1311–1317.
[8] I. Glassman, *Proc. Combust. Inst.* 27 (1998) 1589–1596.
[9] D. Durox, T. Yuan, E. Villermaux, *Combust. Sci. Technol.* 124 (1997) 277–294.
[10] J.L. De Ris, P.K. Wu, G. Heskestad, *Proc. Combust. Inst.* 28 (2000) 2751–2759.
[11] J.L. De Ris, A.M. Kanury, M.C. Yuen, *Proc. Combust. Inst.* 14 (1973) 1033–1042.
[12] L.M. Yuan, G. Cox, *Fire Saf. J.* 27 (1996) 123–139.
[13] S.L. Lee, H.W. Emmons, *J. Fluid Mech.* 11 (1961) 353–368.
[14] Y. Hasemi, M. Nishihata, *Proc. Fire Saf. Sci.* 2 (1988) 275–284.
[15] B. Karlsson, J.G. Quintiere, *Combustion Product, Enclosure Fire Dynamics*, CRC Press, 1999, pp. 228–236 (Chapter 9, Section 3).
[16] International Organization for Standardization. Draft International Standard ISO/DIS 7240-15, Fire Detection and Alarm Systems. Part 15. Point-Type Multisensor (Light and Heat) Fire Detectors, 2002.
[17] L.H. Hu, S. Liu, Y. Xu, D. Li, *J. Combust. Flame* 158 (2011) 586–591.
[18] D. Drysdale, *An Introduction to Fire Dynamics*, second ed., John Wiley and Sons, Chichester, UK, 1998, p. 163.
[19] V.I. Blinov, G.N. Khudiakov, Diffusion Burning of Liquids, AD0296762, *Army Translation*, US, 1961.
[20] B.M. Cetegen, T.A. Ahmed, *Combust. Flame* 93 (1993) 157–184.
[21] E.E. Zukoski, B.M. Cetegen, T. Kubota, *Proc. Combust. Inst.* 20 (1985) 361–366.
[22] P.J. Pagni, *Appl. Mech. Rev.* 43 (1990) 153–170.
[23] B.M. Cetegen, Y. Dong, M.C. Soteriou, *Phys. Fluids* 10 (1998) 1658–1665.
[24] G. Heskestad, *Fire Plumes, SFPE Handbook of Fire Protection Engineering*, second ed., National Fire Protection Association, Quincy, MA, 1995.
[25] A. Hamins, M. Klassen, J. Gore, T. Kashiwagi, *Combust. Flame* 86 (1991) 223–228.